ACS OMEGA

http://pubs.acs.org/journal/acsodf

Article

First-Principles Calculations with Six Structures of Alkaline Earth Metal Cyanide $A(CN)_2$ (A = Be, Mg, Ca, Sr, and Ba): Structural, Electrical, and Phonon Properties

Pak Kin Leong, Toshimori Sekine, Kuan Vai Tam, Sok I. Tam, and Chi Pui Tang*

Cite This: *ACS Omega* 2023, 8, 2973−2981

Read Online

ACCESS | Metrics & More | Article Recommendations | Supporting Information

ABSTRACT: This work examines six structures ($P\bar{4}3m$, $P4_2nm$, $R3m$, $P2_1/c$, $R\bar{3}m$, and $C2/m$) of alkaline earth metal cyanide $A(CN)_2$ (A = Be, Mg, Ca, Sr, and Ba) using first-principles calculations. The symmetries of $P\bar{4}3m$, $P4_2nm$, and $R3m$ reflect a variation of $Pn\bar{3}m$, previously reported as occurring on $Be(CN)_2$ and $Mg(CN)_2$ in X-ray diffraction studies, while the symmetries of $P2_1/c$, $R\bar{3}m$, and $C2/m$ were selected from the $P\bar{3}m1$ symmetry found using $Mg(OH)_2$ as the initial structures, with −OH being replaced by −CN. The band structure, density of states, and phonon properties of all $A(CN)_2$ structures were then investigated using density functional theory (DFT), with a generalized gradient approximation (GGA) applied for the exchange and correlation energy values. The simulation results for the phonon spectra indicate that the stable structures are $Be(CN)_2$ ($P\bar{4}3m$, $P4_2nm$, and $C2/m$), $Mg(CN)_2$ ($P\bar{4}3m$, $P4_2nm$, and $C2/m$), $Ca(CN)_2$ ($P2_1/c$), $Sr(CN)_2$ ($P2_1/c$ and $R\bar{3}m$), and $Ba(CN)_2$ ($R\bar{3}m$) at 0 GPa. For the effects of high pressure, $Ca(CN)_2$ and $Sr(CN)_2$ were thus found to be stable as $C2/m$ at pressures above 10 and 3 GPa, respectively, while $Ca(CN)_2$ is as stable as $R\bar{3}m$ above 15 GPa. In the calculated band structures, all of the compounds with the $C2/m$ structure demonstrated good conductivity, while the other structures have a band gap range of 2.83−6.33 eV.

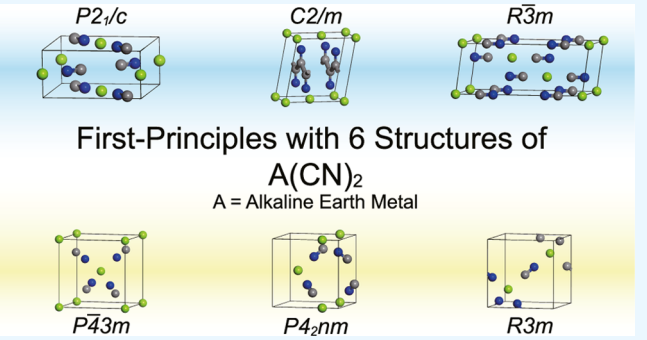

INTRODUCTION

Compounds of the form AX_2, where A and X are the divalent cation and anion, respectively, are very popular in chemistry and have thus been subjected to many studies.[1] Oxides, fluorides, sulfides, hydrides, borides, and hydrates are well-known AX_2 compounds, and the various structures of these have been investigated by means of both intensive experiments[1−4] and theoretical simulations.[5−8] Such examinations of the properties and structural variations of oxides, including their forms at high pressures, provide critical information for the understanding of planetary interiors and industrial materials, for example. Compounds with X = CN, however, are not well known or commonly used due to their limited stabilities[9] and varying bonding natures.[6] Cyanide plays an important role in industrial materials and catalysts for chemical synthesis.[10,11] Metal cyanide-based porous materials have recently been gradually developed.[12,13] Cyanide ligands act as bridging linkers to create various porous coordination polymers (PCP) or metal−organic frameworks (MOFs) depending on the different metals and their coordination numbers. They might be used in energy storage and gas molecule adsorption and may have special features like negative thermal expansion (NTE) and have applications in gas molecular adsorptions and energy storage. Cyanides of $Be(CN)_2$ and $Mg(CN)_2$ have four valence electrons on average, being isoelectronic to diamond, while alkali metal monocyanides preferentially take π-complex structures, with the exception of lithium.[14] In contrast, trivalent A compounds $A(CN)_3$, where the A cation is boron, aluminum, gallium, indium, or thallium, display large structural pores.[9] The properties of AX_2 (A = Ca, Sr, and Ba) could be changed by X anions due to its bonding variations,[5] and this can be used to model the valence shell electron pair repulsion (VSEPR) seen in alkaline earth compounds. A previous study[5] focused on structural variations in AX_2, where the X was −Li, −BeH, $-BH_2$, $-CH_3$, $-NH_2$, −OH, and −F. In a previous study, however, most studies have focused on the geometry, isomerism, thermodynamics, and infrared spectra properties of $A(CN)_2$ single-molecule,[2,6,9,14,15] monocyanides,[16−22] cyano compounds,[12,23,24] and their related ions.[17,25] With regard to the crystal structure of $A(CN)_2$, the X-ray diffraction (XRD)

Received: September 1, 2022
Accepted: November 18, 2022
Published: January 11, 2023

https://doi.org/10.1021/acsomega.2c05667
ACS Omega 2023, 8, 2973−2981

study has reported on the structures of $Be(CN)_2$ and $Mg(CN)_2$.[9] Moreover, the bonding natures of A−C[26−29] and A−N,[27,30−33] where A is an alkaline earth metal, can change some properties of the materials.

On the other hand, carbon and nitrogen are important volatile-forming elements, alongside the lighter elements oxygen and hydrogen, and these form the major constituents of planetary atmospheres.[34] Many interstellar molecules, like MgNC,[35] MgCN,[36] and HMgNC,[37] have been detected and investigated for their effects on the gas phase and dust grain surfaces. The molecular compositions of alkaline earth metals, carbon, and nitrogen have been reported in some theoretical studies,[38−40] and their isomer structures, stabilities, and spectroscopic properties were predicted and combined with observations. It could imply that the surface or interior of the planet will include further alkaline earth metal cyanides or related compounds.

In this study, the structural variations and the electrical, band structure, and phonon properties of $A(CN)_2$ compounds, where A is an alkaline earth metal (Be, Mg, Ca, Sr, or Ba), are explored using first-principles calculations; the results are then compared with prior work. We explore the possibility of the $A(CN)_2$ structures in terms of materials with high-performance properties of A−C/N bonds, the structural diversity of AX_2, and the potential of cyanide-based porous materials. Furthermore, high-pressure phase transitions were also detected in $Zn(CN)_2$ based on Raman measurements,[41] as well as changing both A and X and applying higher pressures can thus be used to explore the effects of various chemical bonds on previous studies on AX_2 compounds. Additionally, the effect of pressure on stability was investigated for $A(CN)_2$ compounds.

CALCULATIONS

First-principles calculations were performed based on density functional theory (DFT)[42,43] as implemented in the Cambridge Sequential Total Energy Package (CASTEP) in Materials Studio.[44,45] For the exchange-correlation function, a generalized gradient approximation (GGA) in the form of the Perdew−Burke−Ernzerhof (PBE) functional was considered,[46] and an ultrasoft pseudopotential method was used.[47] The theory levels, including local-density approximation (LDA),[48,49] screened hybrid functional of Heyd, Scuseria, and Ernzerhof (HSE06),[50] Becke, 3-parameter, Lee−Yang−Parr (B3LYP),[51] PBE0,[52] and screened exchange (sX),[53] were performed to calculate the geometry optimization and band structure of $Be(CN)_2$-$P\bar{4}3m$. The results are shown in the Supporting Information. Although the band gap calculated at the GGA level was usually underestimated due to self-interaction error,[46] the lattice parameters of the GGA level are in good agreement with the XRD study.[9] The GGA-PBE was finally chosen to be employed for the following calculation of the functional after taking lattice parameter optimization and calculation time into consideration. The kinetic energy cutoff was set to 630 eV, while to achieve the structural optimization of all systems, the k-point separation was set to 0.04/Å for all calculations in the Brillouin zone, with the Monkhorst−Pack method of the point distribution applied.[54] The Broyden−Fletcher−Goldfarb−Shanno (BFGS) method[55] was also used, with convergence tolerances set to 5.0×10^{-6} eV/atom for energy; 0.01 eV/Å for maximum force; 0.02 GPa for maximum stress; and 5.0×10^{-4} Å for maximum displacement. The phonon spectra were calculated using the finite displacement method, along with the symmetries of $P\bar{4}3m$, $P4_2nm$, and $R3m$, and the variations of $Pn\bar{3}m$ as reported by the XRD study of $Be(CN)_2$ and $Mg(CN)_2$.[9] The symmetries of $P2_1/c$ (or $P4_2/mnm$), $R\bar{3}m$, and $C2/m$ were found using the $P\bar{3}m1$ symmetry of $Mg(OH)_2$[56] as the initial structure of geometry optimization replacing −OH with −CN.

The spin-polarization calculation using formal spin as the initial state was also implemented with GGA-PBE. The results are shown in the Supporting Information, and no spin-polarization is observed in all systems.

All calculated structures are shown at 0 GPa unless otherwise specified. The geometrical structures and other related graphs were produced using the VESTA software package.[57]

RESULTS AND DISCUSSION

Structures of $P\bar{4}3m$, $P4_2nm$, and $R3m$. The $A(CN)_2$ (A = Be, Mg, Ca, Sr, and Ba) structures with $P\bar{4}3m$, $P4_2nm$, and $R3m$ symmetries are shown in Figure 1. The alkaline earth metal atom (A) is located in the center of the tetrahedron, while the vertices of the tetrahedron in $P\bar{4}3m$, $P4_2nm$, and $R3m$ are composed of 4C (or 4N), 2C+2N, and 1C+3N (or 3C +1N), respectively. In addition, all A−C−N−A forms are linear (both ∠ACN and ∠CNA are equal to or close to 180°; see Tables 1 and S2).

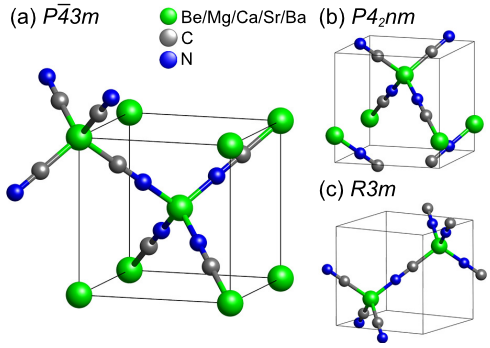

Figure 1. Structures of the $Pn\bar{3}m$ derivative group. (a) $P\bar{4}3m$, (b) $P4_2nm$, and (c) rhombohedral representation of $R3m$. Green, alkaline earth metal; gray, carbon; blue, nitrogen.

The lattice parameters of $P\bar{4}3m$ and $P4_2nm$ $A(CN)_2$ are shown in Table 1 (see Table S2 for $R3m$ $A(CN)_2$). The bond lengths of A−C, A−N, and C−N are shown to be in agreement with both experimental[9] and prior theoretical calculations.[6] Among the three space groups, the lowest cohesive energy is obtained in $P\bar{4}3m$ for $Be(CN)_2$ and $Mg(CN)_2$ and in $P4_2nm$ for the others.

As summarized in Tables 1 and S2 and Figures S9−S11, the band structures show band gaps over 5.3 eV that indicate the presence of insulators. As seen in Figure 2, the phonon spectra of $A(CN)_2$ and all $P\bar{4}3m$ $A(CN)_2$ are dynamically stable, while the characteristic peak of C≡N is red-shifted from 2255 to 2142 cm^{-1} as the atomic number of the alkaline earth metal atom increases.[2,16] Although the $P4_2nm$ forms of $Be(CN)_2$, $Mg(CN)_2$, and $Ca(CN)_2$ (Figure S13) are dynamically stable, other compounds with $P4_2nm$ and $R3m$ symmetries contain soft modes with imaginary frequencies in their phonon spectra (see Figures 3 and S14).

Structures of $P4_2/mnm$ for Be and Mg and $P2_1/c$ for Ca, Sr, and Ba. When optimizing the geometry in the $P2_1/c$

https://doi.org/10.1021/acsomega.2c05667
ACS Omega 2023, 8, 2973−2981

Table 1. Lattice Parameters of $P\bar{4}3m$ (Z = 2) and $P4_2nm$ (Z = 2) $A(CN)_2$[a]

A =	Be		Mg		Ca		Sr		Ba	
space group	$P\bar{4}3m$	$P4_2nm$	$P\bar{4}3m$	$P4_2nm$	$P\bar{4}3m$	$P4_2nm$	$P\bar{4}3m$	$P4_2nm$	$P\bar{4}3m$	$P4_2nm$
$a = b$ (Å)	5.362	5.370	6.235	6.233	6.955	6.953	7.339	7.340	7.753	7.754
	5.339[b]		6.122[b]							
c (Å)	= a	5.378	= a	6.238	= a	6.955	= a	7.338	= a	7.749
V (Å^3)	154.1	155.1	242.4	242.3	336.4	336.3	395.3	395.3	466.0	465.9
	151.2[b]		229.5[b]							
d_{A-C} (Å)	1.784	1.799	2.184	2.181	2.503	2.509	2.669	2.677	2.848	2.858
	1.718[c]		2.108[c]							
	1.644[d]		2.039−2.044[d]		2.377−2.385[d]		2.542−2.588[d]		2.707−2.770[d]	
d_{A-N} (Å)	1.697	1.691	2.049	2.052	2.349	2.342	2.514	2.506	2.692	2.682
	1.522−1.524[d]		1.927−1.928[d]		2.239[d]		2.392−2.409[d]		2.550−2.604[d]	
d_{C-N} (Å)	1.163	1.163	1.167	1.167	1.171	1.172	1.173	1.173	1.174	1.174
	1.187[b]		1.086[b]							
	1.187−1.195[d]		1.188−1.195[d]		1.193−1.198[d]		1.150−1.199[d]		1.150−1.200[d]	
∠ACN (deg)	180.0	179.8	180.0	179.8	180.0	179.9	180.0	179.9	180.0	179.9
∠CNA (deg)	180.0	179.7	180.0	179.9	180.0	179.9	180.0	179.9	180.0	179.9
∠CAC (deg)	109.5	108.9	109.5	109.8	109.5	109.3	109.5	109.4	109.5	109.5
∠NAN (deg)	109.5	110.0	109.5	109.1	109.5	109.6	109.5	109.6	109.5	109.6
E_{coh} (eV)	−7.913	−7.904	−7.521	−7.520	−7.666	−7.667	−7.594	−7.595	−7.622	−7.623
band gap (eV)	6.148	5.937	6.330	6.215	5.759	5.751	5.741	5.733	5.330	5.334
imag. freq.	no	no	no	no	no	no	no	yes	no	yes

[a]E_{coh} is the cohesive energy, while imag. freq. refers to whether there are any imaginary frequencies in the phonon spectrum. [b]XRD experiments by Williams et al.[9] [c]The value is the average of d_{A-C} and d_{A-N} in XRD experiments by Williams et al.[9] [d]Single-molecule calculations by Kapp et al.[6]

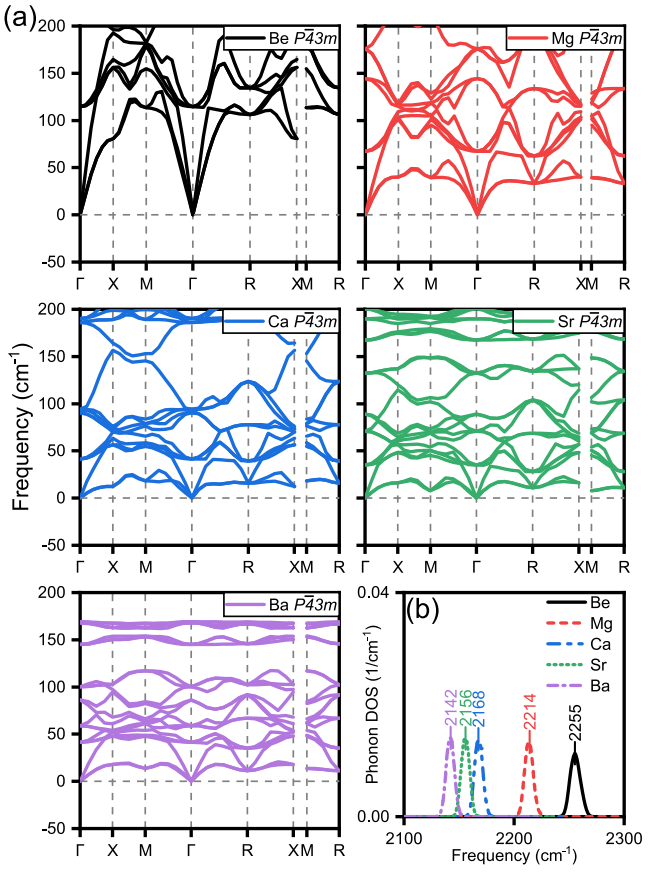

Figure 2. (a) Phonon dispersion spectra of $P\bar{4}3m$ $A(CN)_2$ over the −50 to 200 cm^{-1} wavenumber range. (b) Characteristic peak of C≡N in the phonon density of states (phonon DOS) spectra over the 2100 to 2300 cm^{-1} wavenumber range.

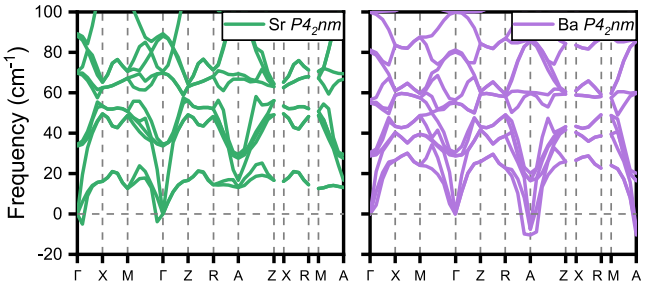

Figure 3. Phonon dispersion spectra of $P4_2nm$ $Sr(CN)_2$ and $Ba(CN)_2$ over the −20 to 100 cm^{-1} wavenumber range.

structure of $Be(CN)_2$ and $Mg(CN)_2$, a higher symmetry was found at $P4_2/mnm$ (Figure 4a) as well as at $P2_1/c$ in $A(CN)_2$ (A = Ca, Sr, and Ba; see Figure 4b).

The lattice parameters of these space groups are shown in Table 2. The C−N bond length of these structures is barely changed relative to that of $P\bar{4}3m$; however, the A−C and A−N

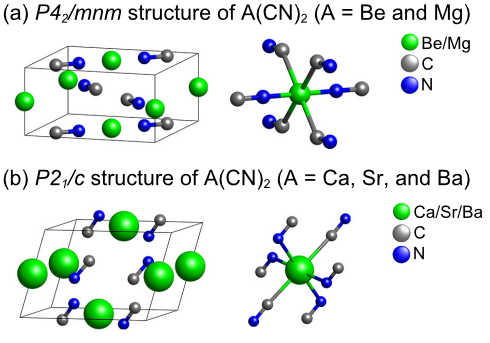

Figure 4. Structures of $A(CN)_2$ (left) and the coordination numbers of A (right). (a) $P4_2/mnm$ for A = Be and Mg. (b) $P2_1/c$ for A = Ca, Sr, and Ba. Colors as in Figure 1.

https://doi.org/10.1021/acsomega.2c05667
ACS Omega 2023, 8, 2973−2981

Table 2. Lattice Parameters of $P2_1/c$ (or $P4_2/mnm$) (Z = 2) $A(CN)_2$

A =	Be	Mg	Ca	Sr	Ba
space group	$P4_2/mnm$			$P2_1/c$	
a (Å)	6.306	7.029	6.267	6.572	6.945
b (Å)	6.306	7.029	4.762	5.079	5.451
c (Å)	3.135	3.380	6.756	7.073	7.411
α (deg)	90.00	90.00	73.57	74.12	75.49
V (Å^3)	124.7	167.0	193.4	227.1	271.6
d_{A-C} (Å)	2.248	2.408	2.583	2.766	2.971
			2.497−2.510[a]	2.678−2.703[a]	2.880−2.975[a]
d_{A-N} (Å)	1.679	2.088	2.491/2.581	2.654/2.714	2.842/2.883
			2.349−2.360[a]	2.512−2.532[a]	2.641−2.725[a]
d_{C-N} (Å)	1.169	1.167	1.178	1.179	1.180
∠ACN (deg)	135.8	135.4	171.7	170.6	170.5
∠CNA (deg)	180.0	180.0	100.8/121.7	104.0/119.6	106.7/117.4
∠CAN (deg)	90.00	90.00	86.57/86.86	84.60/87.12	82.25/88.04
∠NAN (deg)	180.0	180.0	88.85	89.02	89.63
E_{coh} (eV)	−7.528	−7.436	−7.721	−7.680	−7.718
band gap (eV)	2.827	4.746	4.406	4.634	4.579
imag. freq.	yes	yes	no	no	no

[a]Single-molecule calculations by Kapp et al.[6]

bond lengths are longer than those in $P\bar{4}3m$. As the Be−C and Mg−C bond lengths increase more than the others, there seems to be some coordinate bonding between Be/Mg and C. The CN−A−NC (A = Be and Mg) connection is linear, yet the bond length of A−N is shorter than that of A−C. Thus, the Be or Mg atom in this structure is "squashed" to form an octahedron.

The Ca, Sr, or Ba atom in such a structure is octahedrally coordinated with two A−CN linear bonds (∠ACN ≈ 170°) and four A−NC side-on bonds (∠ANC ≈ 100°).

As shown in Table 2, the band gap of $P4_2/mnm$ $Be(CN)_2$ is 2.827 eV, while the others have gaps between 4.406 and 4.746 eV. The phonon spectra of this group are shown in Figures 5 and S16−S18, which also demonstrate that both $P4_2/mnm$ $Be(CN)_2$ and $Mg(CN)_2$ have some imaginary frequencies, while the others are dynamically stable.

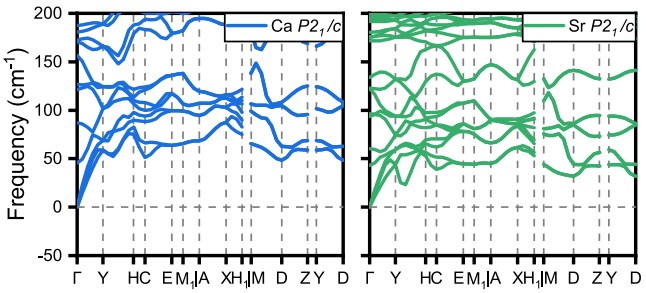

Figure 5. Phonon dispersion spectra of $P2_1/c$ $Ca(CN)_2$ and $Sr(CN)_2$ over the −50 to 200 cm^{-1} wavenumber range.

Structure of $R\bar{3}m$. $R\bar{3}m$ was selected to represent the rhombohedral structure. The main lattice parameters are shown in Table 3. In the rhombohedral structure, as illustrated in Figure 6a, each cyano group is surrounded tetrahedrally by four A atoms, with one A atom linearly bonded with −CN and three A atoms side-on bonded with −NC. When the atomic number of A increases, the angle of the unit cell decreases. The bond lengths of Be−N and Mg−N (3.253 and 2.819 Å, respectively) are thus much longer than those in the other

Table 3. Lattice Parameters of $R\bar{3}m$ (Rhombohedral Representation, Z = 1) $A(CN)_2$

A =	Be	Mg	Ca	Sr	Ba
a (Å)	4.627	4.672	5.163	5.438	5.749
α (deg)	74.05	62.21	53.09	52.06	51.69
V (Å^3)	89.41	75.65	81.55	95.05	108.1
d_{A-C} (Å)	1.676	2.151	2.607	2.796	2.995
d_{A-N} (Å)	3.253	2.819	2.738	2.846	2.999
d_{C-N} (Å)	1.167	1.175	1.182	1.182	1.183
∠ACN (deg)	180.0	180.0	180.0	180.0	180.0
∠CNA (deg)	98.52	98.63	103.4	104.4	105.3
∠ANA (deg)	117.8	117.8	114.8	114.0	113.3
E_{coh} (eV)	−7.312	−7.201	−7.640	−7.656	−7.739
band gap (eV)	4.575	4.772	4.011	4.143	4.122
imag. freq.	yes	yes	yes	no	no

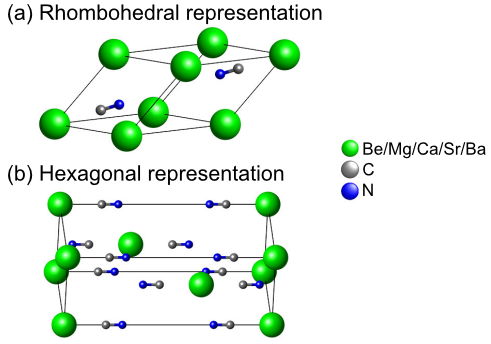

Figure 6. Structure of $R\bar{3}m$ $A(CN)_2$. (a) Rhombohedral representation. (b) Hexagonal representation. Colors as in Figure 1.

space groups, while the bond lengths of Ca−N, Sr−N, and Ba−N are similar to those of the other side-on structures such as $P2_1/c$. In the hexagonal modification as seen in Figure 6b, the structure of NC−A−CN is linear.

The band gap of this group ranges between 4.011 and 4.772 eV, and only $Mg(CN)_2$ has an indirect band gap, with the others demonstrating a direct band gap at the Γ point (Figure S19). Figure 7 shows the phonon dispersion spectra of

https://doi.org/10.1021/acsomega.2c05667
ACS Omega 2023, 8, 2973−2981

$Sr(CN)_2$ and $Ba(CN)_2$; the absence of the imaginary mode indicates that these are dynamically stable at 0 GPa.

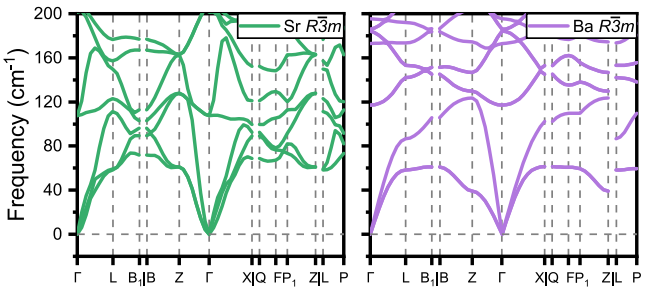

Figure 7. Phonon dispersion spectra of $R\bar{3}m$ $Sr(CN)_2$ and $Ba(CN)_2$ over the −20 to 200 cm^{-1} wavenumber range.

Structure of *C*2/*m*. Figure 8 shows the obtained structure of *C*2/*m* $A(CN)_2$ (A = Be, Mg, Ca, and Sr) using the

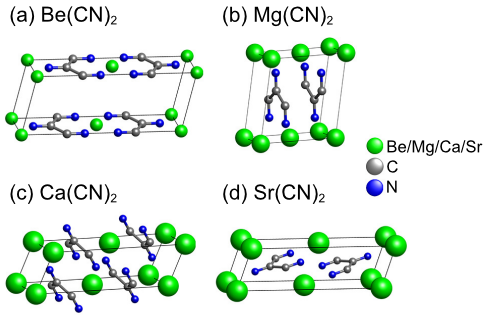

Figure 8. Conventional cell structures of *C*2/*m* $A(CN)_2$. (a–d): A = Be, Mg, Ca, and Sr, respectively. Colors as in Figure 1.

conventional cell. When the *C*2/*m* structure of $Sr(CN)_2$ was modified with the initial *C*2/*m* structure of $Ba(CN)_2$, the space group was changed to $R\bar{3}m$ (see the Structure of R3m section) based on geometric optimization.

The lattice parameters of *C*2/*m* $A(CN)_2$ are shown in Table 4. The bond length of C−N (1.270−1.279 Å) in this structure is elongated significantly, becoming similar to the C−N bond

Table 4. Lattice Parameters of *C*2/*m* (Shown in Primitive Cell, *Z* = 1) $A(CN)_2$

A =	Be	Mg	Ca	Sr
$a = b$ (Å)	5.899	3.174	6.007	6.077
c (Å)	4.531	5.981	3.342	3.538
$\alpha = \beta$ (deg)	82.32	82.88	71.76	74.15
γ (deg)	24.75	50.61	26.49	27.06
V (Å^3)	65.39	46.12	50.93	57.03
d_{A-C} (Å)	3.285	3.153/3.542	3.008/3.211	3.083/3.278
d_{A-N} (Å)	1.741	2.091/2.299	2.422/2.696	2.595/2.770
d_{C-N} (Å)	1.279	1.270	1.269	1.263
d_{C-C} (Å)	1.501	1.598	1.622	1.675
∠ACN (deg)	179.9	165.0	133.1/174.1	133.1/173.0
∠CNA (deg)	133.4	121.5/128.7	91.42/143.3	91.94/144.2
∠ANA (deg)	93.11	80.92	61.39	66.43
∠CCC (deg)	114.8	116.2	116.1	116.2
∠CCN (deg)	122.6	121.9	121.9	121.9
E_{coh} (eV)	−7.835	−7.448	−7.465	−7.316
imag. freq.	no	no	yes	yes

in vinylidendiimine (HN═C═C═NH, d_{C-N} = 1.27 Å),[58] and incorporating an sp^2 hybrid. This type of C−N bond is longer than the normal cyanide bond (about 1.17 Å), and it is noteworthy that the angles of C−C−C and C−C−N are thus closer to 120° to support the sp^2 hybrid model. The C−N in this structure thus differs completely from the standard anion of CN− and the alkaline earth metal coordinates with two adjacent nitrogen atoms.

Figures 9 and S21 show the partial density of states (PDOS) and band structure, and the *C*2/*m* types show conductivity

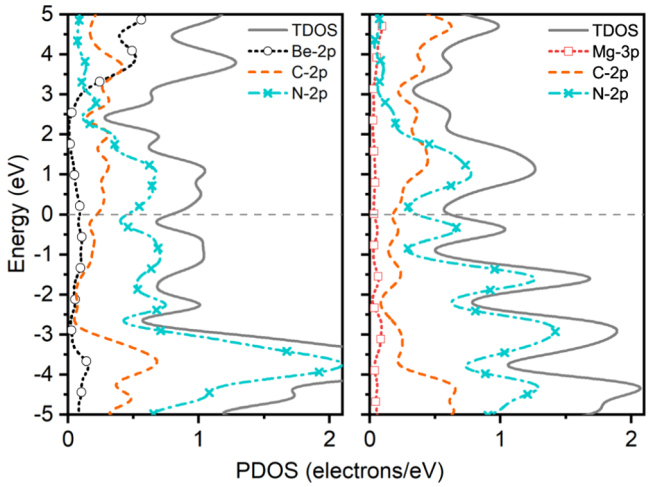

Figure 9. Total density of states (TDOS) and partial density of states (PDOS) of *C*2/*m* $Be(CN)_2$ and $Mg(CN)_2$.

with a contribution consisting of C 2p and N 2p at the Fermi level. This is believed to be due to the conjugated C═N polymerization.

To investigate the dynamical stability, the phonons were calculated with results that indicate that $Be(CN)_2$ and $Mg(CN)_2$ are stable at 0 GPa (Figure 10). The characteristic peak of C═N was also found to red-shift to 1400−1600 cm^{-1} based on the effects of conjugation.

Stability and the Effects of High Pressure. Although the $Pn\bar{3}m$ structure of $Be(CN)_2$ and $Mg(CN)_2$ crystals has

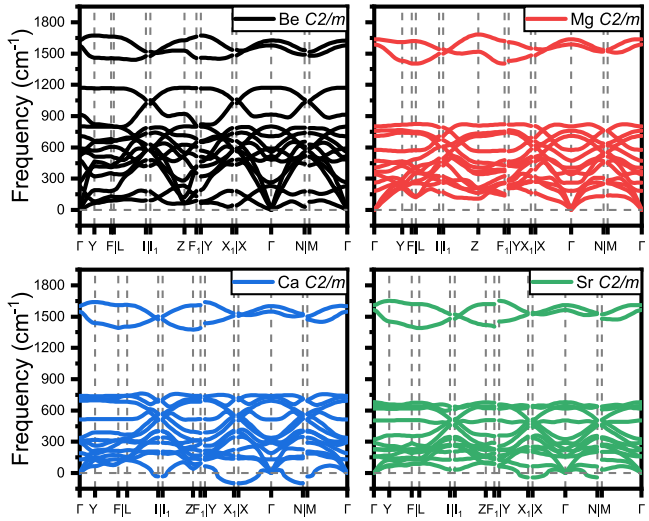

Figure 10. Phonon dispersion spectra of *C*2/*m* $A(CN)_2$ (A = Be, Mg, Ca, and Sr) over the full wavenumber range.

https://doi.org/10.1021/acsomega.2c05667
ACS Omega 2023, 8, 2973−2981

been previously reported, the crystal structures of other alkaline earth metal elements are not well known. This section thus explores the possible ground state of cyanide in conjunction with various alkaline earth metals. The first aspect to consider is thermodynamics. The cohesive energies of structures with different symmetries are compared in Figure 11, which shows that the lowest energy of both $Be(CN)_2$ and

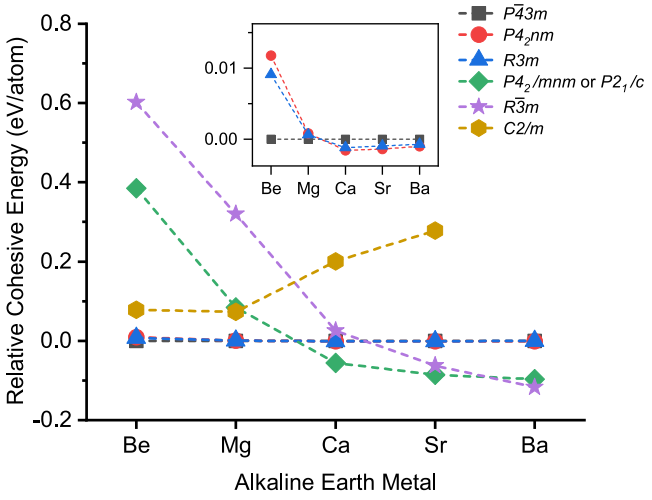

Figure 11. Cohesive energies of $A(CN)_2$ with different symmetries, with $P\bar{4}3m$ set as zero.

$Mg(CN)_2$ is the $P\bar{4}3m$ structure. In this structure, all bonds of A−CN or A−NC are linear, which is beneficial to the formation of $Be(CN)_2$ and $Mg(CN)_2$.[6] The other linear bonding structures (such as $P4_2nm$ and $R3m$) of these two cyanides are also of lower energy than the nonlinear bonding structures (such as $P4_2/mnm$ and $R\bar{3}m$). As the atomic number of A increases, the energies of nonlinear bonding structures sink even lower, with the lowest energy of both $Ca(CN)_2$ and $Sr(CN)_2$ being found in the $P2_1/c$ structure and that of $Ba(CN)_2$ is the $R\bar{3}m$ version.

According to the calculated phonon spectra of all compounds at 0 GPa (summarized in terms of dynamic stability in Tables 1−4 and S2), the ground states of $A(CN)_2$ at 0 GPa appear to be $P\bar{4}3m$, $P\bar{4}3m$, $P2_1/c$, $P2_1/c$, and $R\bar{3}m$, for A = Be, Mg, Ca, Sr, and Ba, respectively.

To investigate the effects of pressure on the stability and property in $Ca(CN)_2$ and $Sr(CN)_2$, the phonons of the $C2/m$ and $R\bar{3}m$ structures at different pressures were calculated. $Ca(CN)_2$ and $Sr(CN)_2$ were thus found to be stable with increasing pressure, with $C2/m$ seen at pressures above 10 and 3 GPa, respectively (Figure 12). $Ca(CN)_2$ was also found to be stable as $R\bar{3}m$, at pressures above 15 GPa (Figure 13).

The cohesive energies were then examined as a function of pressure and compared across the previously described structures, with the results as illustrated in Figures 14 and 15. Figure 14 shows that $Ca(CN)_2$ has a phase transition from $P2_1/c$ to $C2/m$ at a pressure of about 5.5 GPa, alongside a crossing point of two curves representing the $P2_1/c$ and $R\bar{3}m$ structures at about 6 GPa. However, the phonon spectra of $C2/m$ and $R\bar{3}m$ structures reveal that these structures are stable at above 10 GPa, as well as the fact that $Ca(CN)_2$ might exist in a metastable state as $C2/m$ or $R\bar{3}m$. The diagram of $Sr(CN)_2$ shows two phase transition points, at 1 and 9.5 GPa (Figure 15). The first point represents the transition from $P2_1/c$ to $R\bar{3}m$, while the second is from $R\bar{3}m$ to $C2/m$. Unlike $Ca(CN)_2$, the $R\bar{3}m$ structure of $Sr(CN)_2$ is dynamically stable at 0 GPa (Figure 7), while $C2/m$ is stable at 3 GPa (Figure 12). The phase transitions of $Sr(CN)_2$ from $P2_1/c$ to $R\bar{3}m$ and from $R\bar{3}m$ to $C2/m$ may thus occur at higher pressures. In addition, these predicted pressures are in the range of high-

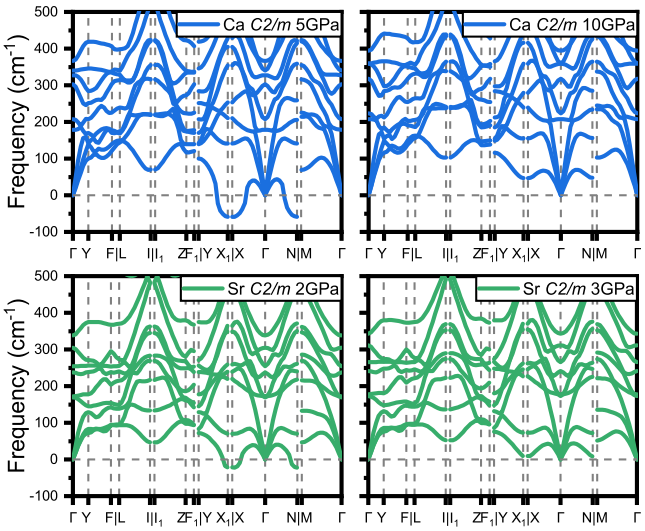

Figure 12. Phonon dispersion spectra of $C2/m$ $Ca(CN)_2$ and $Sr(CN)_2$ over the −100 to 500 cm^{-1} wavenumber range at high pressure.

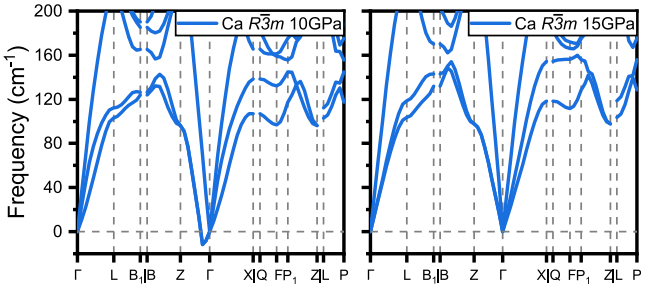

Figure 13. Phonon dispersion spectra of $R\bar{3}m$ $Ca(CN)_2$ over the −20 to 200 cm^{-1} wavenumber range at high pressure.

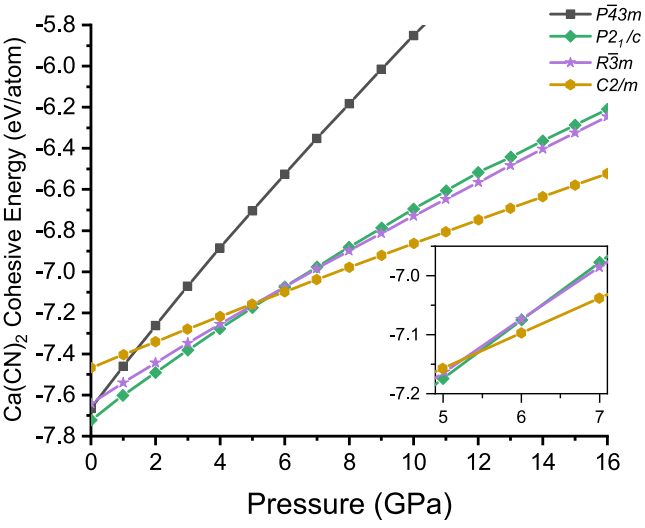

Figure 14. Cohesive energy as a function of pressure with various symmetries of $Ca(CN)_2$.

https://doi.org/10.1021/acsomega.2c05667
ACS Omega 2023, 8, 2973−2981

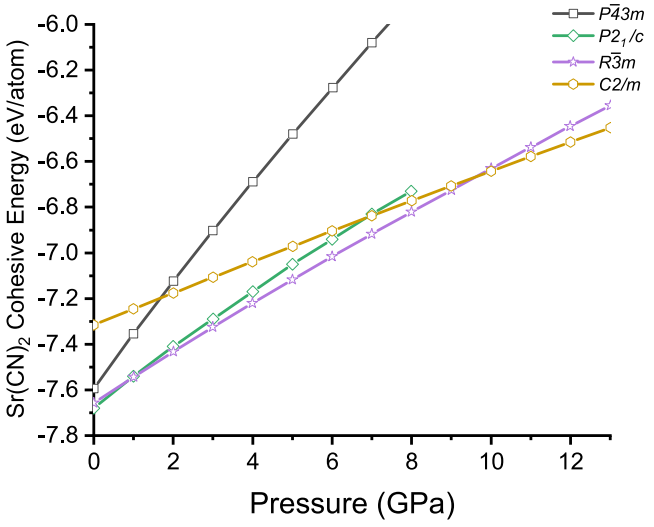

Figure 15. Cohesive energy as a function of pressure with various symmetries of $Sr(CN)_2$, while the calculated $P2_1/c$ structure fails to maintain the symmetry at a pressure higher than 8 GPa.

pressure techniques and it may be possible to synthesize related materials.

CONCLUSIONS

This study used first-principles calculations to examine the lattice structures, band structures, and phonon properties of alkaline earth metal cyanide structures of the form $A(CN)_2$ (A = Be, Mg, Ca, Sr, and Ba) across six symmetries, using GGA to determine DFT. Among the symmetries used, $P2_1/c$, $R\bar{3}m$, and $C2/m$ were reported for $A(CN)_2$, with all results compared with the $Pn\bar{3}m$ series. The results for the bonding between the alkaline earth metal and the cyano group were in good agreement with available theoretical studies.

The band structure calculations thus suggest that the $A(CN)_2$ (A = Be, Mg, Ca, and Sr) structures with $C2/m$ symmetry are conductive.

The $Be(CN)_2$ ($P\bar{4}3m$, $P4_2nm$, and $C2/m$), $Mg(CN)_2$ ($P\bar{4}3m$, $P4_2nm$, and $C2/m$), $Ca(CN)_2$ ($P2_1/c$), $Sr(CN)_2$ ($P2_1/c$ and $R\bar{3}m$), and $Ba(CN)_2$ ($R\bar{3}m$) structures were found to be dynamically stable, based on their phonon dispersion curves. Combined with the results for cohesive energies, it may thus be speculated that the most advantageous structure of $A(CN)_2$ at 0 GPa are $P\bar{4}3m$, $P\bar{4}3m$, $P2_1/c$, $P2_1/c$, and $R\bar{3}m$ (for A = Be, Mg, Ca, Sr, and Ba, respectively).

In terms of the effects of high pressure, $Ca(CN)_2$ ($C2/m$ and $R\bar{3}m$) and $Sr(CN)_2$ ($C2/m$) structures were found to be stable at 10, 15, and 3 GPa. A possible phase transition of $Ca(CN)_2$ and $Sr(CN)_2$ at high pressure was also investigated. These results might suggest the relative ion size effect and the bonding nature of CN^- altering at high pressures.

ASSOCIATED CONTENT

Supporting Information

The Supporting Information is available free of charge at https://pubs.acs.org/doi/10.1021/acsomega.2c05667.

Additional calculated datum (e.g., choice of functional, spin-polarization calculation, lattice parameters of $R3m$ $A(CN)_2$, band structures, density of states, and phonon spectra over full wavenumber range) (PDF).

AUTHOR INFORMATION

Corresponding Author

Chi Pui Tang − *State Key Laboratory of Lunar and Planetary Sciences, Macau University of Science and Technology, Taipa 999078 Macao, China; Faculty of Innovation Engineering, Macau University of Science and Technology, Taipa 999078 Macao, China*; Email: cptang@must.edu.mo

Authors

Pak Kin Leong − *State Key Laboratory of Lunar and Planetary Sciences, Macau University of Science and Technology, Taipa 999078 Macao, China*; orcid.org/0000-0002-8160-8370

Toshimori Sekine − *Center for High Pressure Science and Technology Advanced Research, Shanghai 201203, China*

Kuan Vai Tam − *School of Astronomy and Space Science, Nanjing University, Nanjing 210093, China*; orcid.org/0000-0002-0834-0187

Sok I. Tam − *Faculty of Innovation Engineering, Macau University of Science and Technology, Taipa 999078 Macao, China*; orcid.org/0000-0003-2662-9766

Complete contact information is available at: https://pubs.acs.org/10.1021/acsomega.2c05667

Notes

The authors declare no competing financial interest.

ACKNOWLEDGMENTS

C.P.T., P.K.L., and S.I.T. thank the Science and Technology Development Fund of Macau (FDCT) (Project Nos. 0111/2020/A, 0048/2020/A1, 0105/2020/A3, and 0014/2022/A1) for its support. T.S. thanks the National Natural Science Foundation of China (NSFC) (Grant No. 41974099) for its support.

REFERENCES

(1) Manjón, F. J.; Errandonea, D. Pressure-induced structural phase transitions in materials and earth sciences. *Phys. Status Solidi B* **2009**, *246*, 9−31.

(2) Andrews, L.; Cho, H.-G.; Yu, W.; Wang, X. Matrix Infrared Spectra and Electronic Structure Calculations of Linear Alkaline Earth Metal Di-isocyanides CNMNC, Ionic (NC) M (NC) Bowties, and Ionic (MNC) 2 Rings. *J. Phys. Chem. A* **2019**, *123*, 3743−3760.

(3) Friedrich, A.; Kunz, M.; Miletich, R.; Pattison, P. High-pressure behavior of Ba (OH) 2: phase transitions and bulk modulus. *Phys. Rev. B* **2002**, *66*, No. 214103.

(4) Wong, P. T. T. Pressure-induced splitting and collapsing of the CN stretching vibration band in the Raman spectrum of crystalline Hg (CN) 2. *J. Chem. Phys.* **1984**, *80*, 5937−5941.

(5) Kaupp, M.; Schleyer, P. R. The structural variations of monomeric alkaline earth MX2 compounds (M= calcium, strontium, barium; X= Li, BeH, BH2, CH3, NH2, OH, F). An ab initio pseudopotential study. *J. Am. Chem. Soc.* **1992**, *114*, 491−497.

(6) Kapp, J.; Schleyer, P. R. M (CN) 2 Species (M= Be, Mg, Ca, Sr, Ba): Cyanides, Nitriles, or Neither? *Inorg. Chem.* **1996**, *35*, 2247−2252.

(7) Hatua, K.; Das, H. S.; Mondal, A.; Nandi, P. K. Electronic second hyperpolarizability of alkaline earth metal chains end capped with- NH2 and-CN. *J. Indian Chem. Soc.* **2021**, *98*, No. 100234.

(8) Cazorla, C.; Sagotra, A. K.; King, M.; Errandonea, D. High-pressure phase diagram and superionicity of alkaline earth metal difluorides. *J. Phys. Chem. C* **2018**, *122*, 1267−1279.

(9) Williams, D.; Pleune, B.; Leinenweber, K.; Kouvetakis, J. Synthesis and structural properties of the binary framework C−N

compounds of Be, Mg, Al, and Tl. *J. Solid State Chem.* **2001**, *159*, 244−250.
(10) Gail, E.; Gos, S.; Kulzer, R.; Lorösch, J.; Rubo, A.; Sauer, M.; Kellens, R.; Reddy, J.; Steier, N.; Hasenpusch, W. Cyano Compounds, Inorganic. In *Ullmann's Encyclopedia of Industrial Chemistry*; Wiley-VCH Verlag GmbH & Co. KGaA: Weinheim, 2000.
(11) Wilson, D. W. N.; Urwin, S. J.; Yang, E. S.; Goicoechea, J. M. A Cyaphide Transfer Reagent. *J. Am. Chem. Soc.* **2021**, *143*, 10367−10373.
(12) Chizmeshya, A. V. G.; Ritter, C.; Groy, T.; Tice, J.; Kouvetakis, J. Synthesis of molecular adducts of beryllium, boron, and gallium cyanides: Theoretical and experimental correlations between solid-state and molecular analogues. *Chem. Mater.* **2007**, *19*, 5890−5901.
(13) Xie, Y.; Lin, R.-B.; Chen, B. Old materials for new functions: recent progress on metal cyanide based porous materials. *Adv. Sci.* **2022**, *9*, No. 2104234.
(14) Petrie, S. Magnesium dicyanide: Three isomers or seven? *J. Phys. Chem. A* **1999**, *103*, 2107−2116.
(15) Pickles, C. A.; Toguri, J. Thermodynamic Analysis of the Ca-CN System. *High Temp. Mater. Processes* **2004**, *23*, 405−418.
(16) Lanzisera, D. V.; Andrews, L. Reactions of laser-ablated Mg, Ca, Sr, and Ba atoms with hydrogen cyanide in excess argon. Matrix infrared spectra and density functional calculations on novel isocyanide products. *J. Phys. Chem. A* **1997**, *101*, 9666−9672.
(17) Petrie, S. Trends in M (CN) isomerism: A computational study of monocyanides of the main-group third row atoms. *Phys. Chem. Chem. Phys.* **1999**, *1*, 2897−2905.
(18) Bauschlicher, C. W., Jr.; Langhoff, S. R.; Partridge, H. AB initio study of BeCN, MgCN, CaCN and BaCN. *Chem. Phys. Lett.* **1985**, *115*, 124−129.
(19) Bludský, O.; Špirko, V.; Odaka, T. E.; Jensen, P.; Hirano, T. A theoretical study of the MgNC/MgCN isomerization in the electronic ground state. *J. Mol. Struct.* **2004**, *695*−*696*, 219−226.
(20) Ishii, K.; Hirano, T.; Nagashima, U.; Weis, B.; Yamashita, K. An ab initio prediction of the spectroscopic constants of MgNC-The first Mg-bearing molecule in space. *Astrophys. J.* **1993**, *410*, L43.
(21) Petrie, S. G2 calculations on the thermochemistry of MgCN, MgNC and related species. *J. Chem. Soc., Faraday Trans.* **1996**, *92*, 1135−1140.
(22) Kieninger, M.; Irving, K.; Rivas-Silva, F.; Palma, A.; Ventura, O. N. Density functional and ab initio study of the free radical MgNC. *J. Mol. Struct.: THEOCHEM* **1998**, *422*, 133−141.
(23) Berger, U.; Milius, W.; Schnick, W. Ba2 (CN2)(CN) 2 und Sr2 (CN2)(CN) 2−die ersten gemischten Cyanamid-cyanide. *Z. Anorg. Allg. Chem.* **1995**, *621*, 2075−2082.
(24) Ballmann, G.; Elsen, H.; Harder, S. Magnesium Cyanide or Isocyanide? *Angew. Chem., Int. Ed.* **2019**, *58*, 15736−15741.
(25) Barrientos, C.; Largo, A. Ionization and protonation of (MgCN): an ab initio study of some gas-phase properties of the first magnesium compound in space. *J. Mol. Struct.: THEOCHEM* **1995**, *336*, 29−37.
(26) Rafique, M.; Shuai, Y.; Tan, H.-P.; Hassan, M. Manipulating intrinsic behaviors of graphene by substituting alkaline earth metal atoms in its structure. *RSC Adv.* **2017**, *7*, 16360−16370.
(27) Rafique, M.; Mirjat, N. H.; Soomro, A. M.; Khokhar, S.; Shuai, Y. Manipulation of inherent characteristics of graphene through N and Mg atom co-doping; a DFT study. *Phys. Lett. A* **2018**, *382*, 1108−1119.
(28) Luo, H.; Zhang, L.; Xu, S.; Shi, M.; Wu, W.; Zhang, K. NH3, PH3 and AsH3 adsorption on alkaline earth metal (Be-Sr) doped graphenes: Insights from DFT calculations. *Appl. Surf. Sci.* **2021**, *537*, No. 147542.
(29) Serraon, A. C. F.; Del Rosario, J. A. D.; Chuang, P.-Y. A.; Chong, M. N.; Morikawa, Y.; Padama, A. A. B.; Ocon, J. D. Alkaline earth atom doping-induced changes in the electronic and magnetic properties of graphene: a density functional theory study. *RSC Adv.* **2021**, *11*, 6268−6283.
(30) Muhammad, R.; Shuai, Y.; Tan, H.-P. A first-principles study on alkaline earth metal atom substituted monolayer boron nitride (BN). *J. Mater. Chem. C* **2017**, *5*, 8112−8127.
(31) Rafique, M.; Unar, M. A.; Ahmed, I.; Chachar, A. R.; Shuai, Y. Ab-initio investigations on physisorption of alkaline earth metal atoms on monolayer hexagonal boron nitride (h-BN). *J. Phys. Chem. Solids* **2018**, *118*, 114−125.
(32) Ma, L.-C.; Sun, Y.-R.; Wang, L.-C.; Ma, L.; Zhang, J.-M. Calcium decoration of boron nitride nanotubes with vacancy defects as potential hydrogen storage materials: A first-principles investigation. *Mater. Today Commun.* **2021**, *26*, No. 101985.
(33) Ma, L.; Wang, L.; Sun, Y.; Ma, L.; Zhang, J. First-principles study of hydrogen storage on Ca-decorated defective boron nitride nanosheets. *Physica E* **2021**, *128*, No. 114588.
(34) Grewal, D. S.; Dasgupta, R.; Sun, C.; Tsuno, K.; Costin, G. Delivery of carbon, nitrogen, and sulfur to the silicate Earth by a giant impact. *Sci. Adv.* **2019**, *5*, No. eaau3669.
(35) Kawaguchi, K.; Kagi, E.; Hirano, T.; Takano, S.; Saito, S. Laboratory spectroscopy of MgNC-The first radioastronomical identification of Mg-bearing molecule. *Astrophys. J.* **1993**, *406*, L39−L42.
(36) Ziurys, L. M.; Apponi, A.; Guélin, M.; Cernicharo, J. Detection of MgCN in IRC+ 10216: A new metal-bearing free radical. *Astrophys. J.* **1995**, *445*, L47−L50.
(37) Cabezas, C.; Cernicharo, J.; Alonso, J. L.; Agúndez, M.; Mata, S.; Guelin, M.; Peña, I. Laboratory and astronomical discovery of hydromagnesium isocyanide. *Astrophys. J.* **2013**, *775*, 133.
(38) Vega-Vega, Á.; Largo, A.; Redondo, P.; Barrientos, C. Structure and Spectroscopic Properties of [Mg, C, N, O] Isomers: Plausible Astronomical Molecules. *ACS Earth Space Chem.* **2017**, *1*, 158−167.
(39) Cabezas, C.; Barrientos, C.; Largo, A.; Guillemin, J.-C.; Cernicharo, J.; Alonso, J. L. Alkaline and alkaline-earth cyanoacetylides: A combined theoretical and rotational spectroscopic investigation. *J. Chem. Phys.* **2019**, *151*, No. 054312.
(40) Woon, D. E. Icy Grain Mantle Surface Astrochemistry of MgNC: The Emergence of Metal Ion Catalysis Studied via Model Ice Cluster Calculations. *J. Phys. Chem. A* **2022**, *126*, 5186−5194.
(41) Jain, A. B.; Deb, S.; Tyagi, A. High pressure Raman spectroscopic study of phase transformations in Zn (CN) 2. *Chem. Phys. Lett.* **2020**, *758*, No. 137947.
(42) Hohenberg, P.; Kohn, W. Inhomogeneous electron gas. *Phys. Rev.* **1964**, *136*, B864−B871.
(43) Levy, M. Universal variational functionals of electron densities, first-order density matrices, and natural spin-orbitals and solution of the v-representability problem. *Proc. Natl. Acad. Sci. U.S.A.* **1979**, *76*, 6062−6065.
(44) Segall, M. D.; Lindan, P. J.; Probert, M.; Pickard, C.; Hasnip, P.; Clark, S.; Payne, M. First-principles simulation: ideas, illustrations and the CASTEP code. *J. Phys.: Condens. Matter* **2002**, *14*, 2717.
(45) Clark, S. J.; Segall, M. D.; Pickard, C. J.; Hasnip, P. J.; Probert, M. J.; Refson, K.; Payne, M. First principles methods using CASTEP. *Z. Kristallogr. − Cryst. Mater.* **2005**, *220*, 567−570.
(46) Perdew, J. P.; Burke, K.; Ernzerhof, M. Generalized gradient approximation made simple. *Phys. Rev. Lett.* **1996**, *77*, 3865.
(47) Vanderbilt, D. Soft self-consistent pseudopotentials in a generalized eigenvalue formalism. *Phys. Rev. B* **1990**, *41*, 7892.
(48) Ceperley, D. M.; Alder, B. J. Ground state of the electron gas by a stochastic method. *Phys. Rev. Lett.* **1980**, *45*, 566.
(49) Perdew, J. P.; Zunger, A. Self-interaction correction to density-functional approximations for many-electron systems. *Phys. Rev. B* **1981**, *23*, 5048.
(50) Krukau, A. V.; Vydrov, O. A.; Izmaylov, A. F.; Scuseria, G. E. Influence of the exchange screening parameter on the performance of screened hybrid functionals. *J. Chem. Phys.* **2006**, *125*, No. 224106.
(51) Becke, A. D. Density-functional thermochemistry. 3. The role of exact exchange. *J. Chem. Phys.* **1993**, *98*, 5648−5652.
(52) Adamo, C.; Barone, V. Toward reliable density functional methods without adjustable parameters: The PBE0 model. *J. Chem. Phys.* **1999**, *110*, 6158−6170.

https://doi.org/10.1021/acsomega.2c05667
ACS Omega 2023, 8, 2973−2981

(53) Seidl, A.; Görling, A.; Vogl, P.; Majewski, J. A.; Levy, M. Generalized Kohn-Sham schemes and the band-gap problem. *Phys. Rev. B* **1996**, *53*, 3764.
(54) Monkhorst, H. J.; Pack, J. D. Special points for Brillouin-zone integrations. *Phys. Rev. B* **1976**, *13*, 5188.
(55) Pfrommer, B. G.; Cote, M.; Louie, S. G.; Cohen, M. L. Relaxation of crystals with the quasi-Newton method. *J. Comput. Phys.* **1997**, *131*, 233−240.
(56) Hermann, A.; Mookherjee, M. High-pressure phase of brucite stable at Earth's mantle transition zone and lower mantle conditions. *Proc. Natl. Acad. Sci. U.S.A.* **2016**, *113*, 13971−13976.
(57) Momma, K.; Izumi, F. VESTA 3 for three-dimensional visualization of crystal, volumetric and morphology data. *J. Appl. Crystallogr.* **2011**, *44*, 1272−1276.
(58) Cignitti, M.; Tosato, M. The relative stabilities of isomeric HCN dimers. *Bioelectrochem. Bioenerg.* **1977**, *4*, 98−103.

https://doi.org/10.1021/acsomega.2c05667
ACS Omega 2023, 8, 2973−2981